Liu, X., Zhang, X., Liu, S., Liu, J., and Chen, Q. "Optimization of multi-V filter design for airliner environmental control system using an empirical model," *Separation and Purification Technology,* 257: 117966.

Optimization of multi-V filter design for airliner environmental control system using an empirical model

Xuan Liu[a], Xin Zhang[a], Sumei Liu[a,b*], Junjie Liu[a], Qingyan Chen[b]

[a]*Tianjin Key Lab of Indoor Air Environmental Quality Control, School of Environmental Science and Engineering, Tianjin University, Tianjin 300072, China*

[b]*School of Mechanical Engineering, Purdue University, West Lafayette, IN 47907, USA*

** Corresponding author email: smliu@tju.edu.cn*

HIGHLIGHTS

- Establishment of empirical equation for pressure drop across multi-V cabin filter.
- Measurements of pressure drop across various multi-V cabin filters for verification of the empirical equation.
- Development of two optimized design procedures for multi-V HEPA filters and comparison with actual parameters.

ABSTRACT

With the wide use of multi-V filters in aircraft cabins, it is necessary to establish a pressure drop prediction and optimization model for multi-V HEPA cabin filters. Based on approximate solution of the Navier-Stokes equation and with the aid of CFD simulations, we developed an empirical equation for the overall pressure drop across a multi-V HEPA cabin filter. The measured pressure drop across the filter was used to verify the accuracy of the empirical equation. The equation was then used to develop two optimized design procedures for multi-V HEPA cabin filters with low pressure drop and high filtration efficiency. The structural parameters of the filters obtained by the two design procedures were consistent and very close to the actual parameters. Compared with CFD, this empirical equation is easier to use and involves only a short calculation time. The empirical equation and optimized design procedures are useful for filter design.

Keywords: Pressure drop, Empirical equation, Optimal design, HEPA filter

Nomenclature

A	area, m^2
Da	Darcy number
f_{1-6}	auxiliary function
H	channel width of pleat, m
k	permeability, m^2
L	pleat height, m
Δp	pressure drop, Pa
Q	flow rate, m^3/h
Re	Reynolds number

s	medium thickness, m
U	face velocity of mini-pleat panel, m/s
v, V	velocity, m/s
x, y	Cartesian coordinates
Y	pleat spacing, m

Greek letters

β	pleat height/pleat spacing ratio
μ	fluid viscosity, $\mathrm{N \cdot s/m^2}$
ξ	local resistance coefficient
ρ	fluid density, $\mathrm{kg/m^3}$
φ	the angle between the pleats

Subscripts

cs	cross sectional
dw	downwind
in	filter inlet
m	filter medium
mp	mini-pleat flow channel
out	filter outlet
t	total
uw	upwind
vp	flow channel between the V-panels
x, y	Cartesian coordinates
0	indicates V-panel parameters

Symbols

*	dimensionless quantity
< >	quantity averaged across the gap width

1. Introduction

Large amounts of particulate matter (PM) can be found in airliner cabins, emitted by passengers and crew members as they cough [1, 2], talk [1] and breathe [3], from chemical reactions between passengers and ozone [4, 5], and from outdoor air pollution [6, 7]. Exposure to PM has an adverse impact on human health [8]. PM_{10} can enter the respiratory system, and $PM_{2.5}$ can even enter the blood circulation system through the alveoli [9]. Particulate matter can thus increase the morbidity and mortality of respiratory and cardiovascular diseases [10]. In addition, freshly emitted ultrafine particulates from airliner exhausts could damage DNA by creating an imbalance between oxidation and antioxidation [11]. Aerosol or airborne transmission of various diseases, such as tuberculosis, measles, chickenpox and SARS, has been widely recognized [12]. The COVID-19 illness can be transmitted between people through respiratory droplets [13], which increases passengers' concern about possible spread of the virus in airliner cabins.

To reduce the exposure of passengers to pollutants, the environmental control systems of most commercial aircraft are equipped with high-efficiency particulate air (HEPA) filters [14] as required by ANSI/ASHRAE Standard 161 [15]. HEPA filters are essential to the safety, comfort, and health of passengers and crew members. ASHRAE Standard 161 [15] requires aircraft cabin filters to have a filtration efficiency of ≥ 99.97% for 0.3 μm or larger particles. Some filters [16] can also remove gaseous pollutants. At the same time, the standard of cabin filter BS EN ISO 29463-5 [30] stated that the initial pressure drop value of the filter was one of the important indicators to judge the performance of the filter. In addition, according to the requirements of different aircraft manufacturers, the replacement cycle for cabin filters ranges from 3600 to 6000 hours without intermediate testing. Therefore, the HEPA filters used in commercial airplanes must be able to handle a large volume flow of air, and maintain a low pressure drop and high filtration efficiency for their entire service life.

At present, the main types of filters used in commercial aircraft are the multi-V filter, pleated filter panel, and cartridge filter. The multi-V filter is the most widely used in cabin filtration, installed in almost all Boeing airplane models. The filter consists of multiple mini-pleat panels as shown in Fig. 1. With the same external dimensions, this multi-V filter has a larger filtration area than the pleated filter panel, and can better adapt to an environment requiring a high air volume flow rate and high dust-holding capacity. The increase in filtration area reduces the filtration velocity, which not only improves the particle collection efficiency but also reduces the pressure drop. The cartridge filter also has the advantages of large filtration area per unit volume, low pressure drop, and high dust holding capacity, but it is only used in some Airbus models.

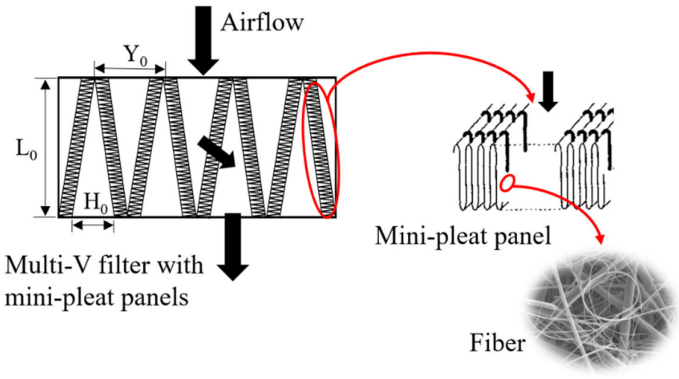

Fig. 1. Schematic of a multi-V filter

To design low-pressure-drop pleated filter panels, many researchers have optimized the structure through experiments or simulations [17-21]. CFD simulation can accurately depict the flow field between filter pleats, and it can be used to optimize filtration performance by analyzing the main factors affecting the total pressure drop. However, the simulation requires the establishment of physical models with different parameters and mesh them, which entails a long computing time. It is very tedious

and time-consuming to optimize the filter structure by CFD, especially for multi-V filters with a complex structure.

Meanwhile, a number of studies have used empirical models to predict and optimize the pressure drop across pleated filter panels. Yu and Goulding [22] applied the Navier-Stokes equation to the pleat channel, and established a semi-analytical calculation of pressure drop for HEPA pleated filters. Lücke and Fissan [23] established a simplified model of the pressure drop across pleated filter panels based on the approximate solution of the Navier-Stokes equation. The model's calculation agreed with the corresponding experimental and simulated results. Chen et al. [24] analyzed experimental data on filter pressure drop and proposed a semi-empirical model which is suitable for triangular pleat structure. Rebaï et al. [25] proposed a semi-analytical model for a pleated filter used in automobiles. Their comparison with experimental data showed that the model could be used to determine the optimal pleated density. Meanwhile, some studies used experimental data to mathematically analyze the filter pressure drop and geometric parameters, establishing a dimensionless model [18] and an empirical two-parameter correlation [19]. Most of the empirical models above were based on the Navier-Stokes equation, but very few studies addressed the multi-V filter.

Therefore, the objectives of this paper were (1) to develop an empirical equation for pressure drop across a multi-V filter, (2) to use experimental data on multi-V filter pressure drop to verify the accuracy of the empirical equation, and (3) to identify an optimal design method for the multi-V filter using the empirical equation. This paper reports the results we obtained.

2. Method

2.1 Method of establishing the empirical equation

The pressure drop across a multi-V filter is the most important design parameter. The pressure drop consists of five parts:

$$\Delta p_t = \Delta p_{in} + \Delta p_{out} + \Delta p_{vp} + \Delta p_{mp} + \Delta p_m \quad (1)$$

where Δp_t is total pressure drop, Δp_{in} filter inlet pressure drop, Δp_{out} filter outlet pressure drop, Δp_{vp} the pressure drop in the flow channel between V-panels, Δp_{mp} the pressure drop in the mini-pleat flow channel, and Δp_m the pressure drop across the filter medium. The sum of Δp_{in}, Δp_{out}, and Δp_{vp} is the pressure drop caused by the V-panel structure.

For HEPA pleated filters, the flow between pleats is generally considered to be laminar [17, 22, 23]. Some methods are limited to the special case of rectangular pleats [17, 22]. The algorithm proposed by Lücke and Fissan [23] applies to both triangular and rectangular pleats. This investigation used their algorithm together with CFD to accurately simulate the flow field in pleats, in order to solve the pressure drop in the mini-pleat flow channel Δp_{mp}. Since the structures of mini-pleats and V-panels are similar, we modified the solution method of Δp_{mp} to find Δp_{vp}. Our aim was an empirical model for pressure drop across multi-V cabin filters.

To develop an empirical equation for solving Δp_{mp}, the following dimensionless parameters are first normalized by the face velocity (U) of the mini-pleat panel and the mini-pleat spacing (Y) as shown in Fig. 2.

$$p^* = \frac{p}{\rho U^2}, \quad v_x^* = \frac{v_x}{U}, \quad v_y^* = \frac{v_y}{U}, \quad x^* = \frac{x}{Y},$$

$$y^* = \frac{y}{Y}, \quad s^* = \frac{s}{Y}, \quad \beta = \frac{L}{Y}, \quad H^* = \frac{H}{Y}.$$

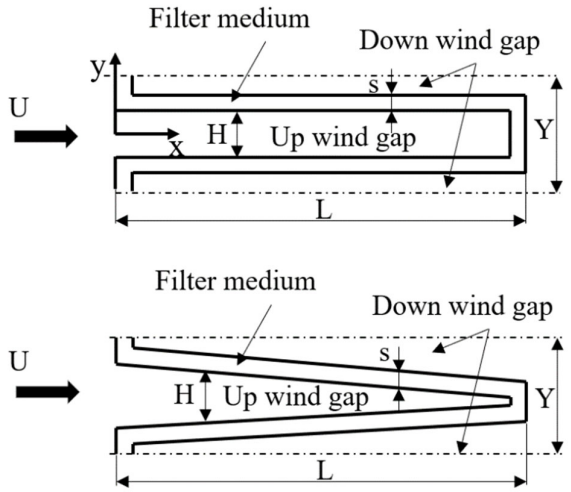

Fig. 2. Definition of key parameters for rectangular and triangular pleats.

The flow through a multi-V filter is governed by the Navier-Stokes equation, which can be expressed as follows in the x direction (along the centerline of the gap):

$$v_x^* \frac{\partial v_x^*}{\partial x^*} + v_y^* \frac{\partial v_x^*}{\partial y^*} = -\frac{\partial p^*}{\partial x^*} + \frac{1}{Re}\left(\frac{\partial^2 v_x^*}{\partial x^{*2}} + \frac{\partial^2 v_x^*}{\partial y^{*2}}\right) \tag{2}$$

$$Re = \frac{\rho U Y}{\mu}$$

Eq. (2) can be averaged across the gap width by introducing an average local quantity:

$$\langle z(x^*) \rangle = \frac{2}{H^*(x^*)} \int_0^{(1/2)H^*(x^*)} z(x^*, y^*)\, dy^* \tag{3}$$

to yield the average pressure gradient equation:

$$\frac{d\langle p^* \rangle}{dx^*} = \frac{1}{Re} \frac{d^2 \langle v_x^* \rangle}{dx^{*2}} + \frac{2}{ReH^*} \left[\frac{\partial v_x^*}{\partial y^*}\right]_{y^*=0}^{y^*=(1/2)H^*} - \frac{1}{2} \frac{d\langle v_x^{*2} \rangle}{dx^*}$$

$$- \frac{2}{H^*} \int_0^{\left(\frac{1}{2}\right)H^*} v_y^* \frac{\partial v_x^*}{\partial y^*} dy^* \tag{4}$$

The average pressure difference between the inlet and outlet of the mini-pleat downstream gap is the pressure drop in the mini-pleat flow channel Δp_{mp} [23, 26]. Because the medium is heavily compressed at the top of the pleat during the pleating

process, only a small amount of fluid enters the pleat at the top, and thus the boundary condition $\langle v_x^*(x^* = s^*)\rangle = 0$ is used. In practice, s^* is far less than β, and Eq. (4) (starting from $x^* = 0$) can be integrated to form:

$$\Delta p_{mp}^* = \langle p^*(x^* = 0)\rangle_{dw} - \langle p^*(x^* = \beta)\rangle_{dw} = -\int_0^{\beta} \frac{d\langle p^*\rangle_{dw}}{dx^*} dx^* \tag{5}$$

To solve Eqs. (4) and (5) for obtaining Δp_{mp}^*, it is necessary to find $\langle v_x^*\rangle_{dw}$, $v_{x,dw}^*$ and $v_{y,dw}^*$.

When the law of conservation of mass is applied to the finite element of the downwind gap, $\langle v_x^*\rangle_{dw}$ can be solved:

$$\frac{1}{2} H_{dw}^* \langle v_x^*\rangle_{dw} + v_m^* \frac{1}{\cos\varphi} \delta x^* = \frac{1}{2} H_{dw}^* \langle v_x^*\rangle_{dw} + \frac{d}{dx^*}\left(\frac{1}{2} H_{dw}^* \langle v_x^*\rangle_{dw}\right) \delta x^* \tag{6}$$

where φ is the angle between the surface of the medium and the centerline of the gap, and v_m^* is the filter medium velocity. After simplification and integration, we have the following equation:

$$\langle v_x^*\rangle_{dw} = \frac{2}{H_{dw}^*} \int_0^{x^*} v_m^* \cos\varphi \, dx \tag{7}$$

We used CFD to simulate the pleat field between folds in order to obtain the mathematical expression of $v_{x,dw}^*$ and $v_{y,dw}^*$. The simulation method is described in detail in Section 2.2. Using the simulation results as shown in Section 3.1, we can develop the expression of $v_{x,dw}^*$ and $v_{y,dw}^*$.

The form of the x-direction velocity component produced by the CFD simulations was consistent with the assumption made by Lücke and Fissan [23]. Both show that the x-component velocity can be expressed as a quadratic polynomial:

$$v_x^*(x^*, y^*) = v_{x,max}^*(x^*)\left[1 + f_1(x^*)\left(\frac{2y^*}{H^*(x^*)}\right) + f_2(x^*)\left(\frac{2y^*}{H^*(x^*)}\right)^2\right] \tag{8}$$

According to the characteristics of x-component velocity in the Fig. 6, further assumptions are listed as follows:

(1) The maximal x-velocity occurs along the centerlines of the gaps, namely:

$$v_x^*(x^*, y^* = 0) = v_{x,max}^*(x^*) \tag{9}$$

(2) The velocity profile is symmetric:

$$\frac{\partial v_x^*(x^*, y^* = 0)}{\partial y^*} = 0 \tag{10}$$

(3) It can be easily seen from the simulation results that v_x is zero at the filter medium, but v_y is the largest. So, the fluid enters and escapes from the medium's surface perpendicularly:

$$v_x^*\left(x^*, y^* = \frac{1}{2} H^*\right) = v_m^* \sin\varphi. \tag{11}$$

Therefore,

$$v_{x,dw}^{*} = \frac{3}{2}\langle v_x^{*}\rangle_{dw} - \frac{1}{2}v_m^{*}sin\varphi + \left(\frac{3}{2}v_m^{*}sin\varphi - \frac{3}{2}\langle v_x^{*}\rangle\right)\left(\frac{2y^{*}}{H_{dw}^{*}}\right)^{2} \quad (12)$$

For $v_{y,dw}^{*}$, the CFD simulations showed that the y-component velocity is a typical cubic function, rather than the special quadratic function form used by Lücke and Fissan [23]. Then the y-component of the velocity field can be expressed as a cubic polynomial:

$$v_{y,dw}^{*}(x^{*},\, y^{*}) = f_3(x^{*})\left(\frac{2y^{*}}{H_{dw}^{*}(x^{*})}\right)^{3}$$

$$+ f_4(x^{*})\left(\frac{2y^{*}}{H_{dw}^{*}(x^{*})}\right)^{2} + f_5(x^{*})\left(\frac{2y^{*}}{H_{dw}^{*}(x^{*})}\right) \quad (13)$$

Similarly, according to the characteristics of y-component of the velocity in the Fig. 6, we assume further:

(1) The y-velocity at the centerlines of the gaps is zero:

$$v_y^{*}(x^{*},\, y^{*} = 0) = 0 \quad (14)$$

(2) The fluid enters and escapes from the medium surface perpendicularly:

$$v_y^{*}\left(x^{*},\, y^{*} = \frac{1}{2}H_{dw}\right) = -v_m^{*}cos\varphi \quad (15)$$

$$v_y^{*}\left(x^{*},\, y^{*} = -\frac{1}{2}H_{dw}\right) = v_m^{*}cos\varphi \quad (16)$$

(3) The conservation of mass has to be fulfilled:

$$-\frac{\partial v_x^{*}(x^{*},\, y^{*})}{\partial x^{*}} = \frac{\partial v_y^{*}(x^{*},\, y^{*})}{\partial y^{*}} \quad (17)$$

A severe problem is the determination $f_3(x^{*})$ from the conservation of mass. If the function $f_3(x^{*})$ depends on x^{*} only, it is impossible to fulfill the conservation of mass everywhere. This is because we found that $f_3(x^{*})$ derived by calculation still contains y^{*}. This is in conflict with the basic form of Eq. (13), where $f_3(x^{*})$is supposed to be independent from y^{*}. So, that the conservation of mass is exactly fulfilled only in the middle of the gap (y^{*} = 0) [23].

Thus,

$$v_{y,dw}^{*} = \left(\frac{3}{4}H_{dw}^{*}\frac{d\langle v_x^{*}\rangle_{dw}}{dx^{*}} - v_m^{*}cos\varphi\right)\left(\frac{2y^{*}}{H_{dw}^{*}}\right)^{3} - \frac{3}{4}H_{dw}^{*}\frac{d\langle v_x^{*}\rangle_{dw}}{dx^{*}}\left(\frac{2y^{*}}{H_{dw}^{*}}\right) \quad (18)$$

In the case of a low-permeability filter medium, previous studies demonstrated that the medium velocity v_m^{*} was constant [18, 20, 27]. According to the law of mass conservation, $v_m^{*} = 1/2\beta$. For a rectangular pleat with H^{*}as a constant ($\varphi = 0$):

$$\langle v_x^{*}\rangle_{dw} = \frac{x^{*}}{H\beta} \quad (19)$$

$$v_{x,dw}^{*} = \frac{3}{2}\frac{x^{*}}{H^{*}\beta}\left[1 - \left(\frac{2y^{*}}{H^{*}}\right)^{2}\right] \quad (20)$$

$$v_{y,dw}^{*} = \left(\frac{1}{4\beta}\right)\left(\frac{2y^{*}}{H^{*}}\right)^{3} - \frac{3}{4\beta}\frac{2y^{*}}{H^{*}} \tag{21}$$

For a triangular pleat with $H^{*} = 2x^{*}\,tan\,\varphi$

$$\langle v_{x}^{*}\rangle_{dw} = \frac{1}{2\beta\,\sin\varphi} \tag{22}$$

$$v_{x,dw}^{*} = \frac{3}{4\beta\,sin\,\varphi} - \frac{sin\,\varphi}{4\beta} + \left(\frac{3\,sin\,\varphi}{4\beta} - \frac{3}{4\beta\,sin\,\varphi}\right)\left(\frac{2y^{*}}{2x^{*}\,tan\,\varphi}\right)^{2} \tag{23}$$

$$v_{y,dw}^{*} = -\frac{\cos\varphi}{2\beta}\left(\frac{2y^{*}}{2x^{*}\tan\varphi}\right)^{3} \tag{24}$$

Combining $\langle v_{x}^{*}\rangle_{dw}$, $v_{x,dw}^{*}$ and $v_{y,dw}^{*}$ of the rectangular pleat with Eqs. (4) and (5):

$$\Delta p_{mp} = \left(\frac{6\beta}{ReH^{*3}} + \frac{6}{5H^{*2}}\right)\rho U^{2} \tag{25}$$

With the non-dimensional form of Darcy's law, the pressure drop across the filter medium is:

$$\Delta p_{m} = \frac{s^{*}}{2Da\beta}\rho U^{2} \quad Da = \frac{k\rho U}{\mu Y} \tag{26}$$

Therefore, the pressure drop across the mini-pleat panel can be expressed as:

$$\Delta p_{mp} + \Delta p_{m} = \left(\frac{6\beta}{ReH^{*3}} + \frac{6}{5H^{*2}} + \frac{s^{*}}{2Da\beta}\right)\rho U^{2} \tag{27}$$

The face velocity of a mini-pleat panel is the ratio of the airflow rate and the mini-pleat panels' windward area. This formula can also be used to solve the pressure drop across pleated filter panels.

At the same time, the V-panel parameters are used to derive the pressure drop in the flow channel between the V-panels, Δp_{vp}. Fig. 1 provides the definitions of several important parameters. The following dimensionless parameters are introduced with the use of filter inlet velocity (V_{in}) and mini-pleat panel spacing (Y_0):

$$p_{0}^{*} = \frac{p_{0}}{\rho {V_{1}}^{2}}, \quad s_{0}^{*} = \frac{L}{Y_{0}}, \quad \beta_{0} = \frac{L_{0}}{Y_{0}}, \quad Re_{0} = \frac{\rho V_{in} Y_{0}}{\mu}.$$

The V-panels are simplified into ideal triangular pleats in the solution process. Next, the above parameters are brought into $\langle v_{x}^{*}\rangle_{dw}$, $v_{x,dw}^{*}$ and $v_{y,dw}^{*}$ of the triangular pleat (Eqs. (22) through (24)), and Eq. (5) is used to calculate Δp_{vp}. It was found that for ideal triangular pleats, if the integral starts from $x^{*} = 0$, the denominator will be zero; thus, the integral should start from $x^{*} = \frac{s_{0}^{*}}{\sin\varphi_{0}}$. The other conditions are the same as above, and the result is:

$$\Delta p_{vp} = \left(\frac{3(\sin^{2}\varphi_{0} - 1)}{2\beta_{0}\tan\varphi_{0}\sin\varphi_{0}}\left(\frac{\beta_{0}\sin\varphi_{0} - s_{0}^{*}}{s_{0}^{*}\beta_{0}\tan\varphi_{0}\,Re_{0}} + \frac{\cos\varphi_{0}}{10\beta_{0}}\ln\frac{\sin\varphi_{0}\,\beta_{0}}{s_{0}^{*}}\right)\right)\rho {V_{in}}^{2} \tag{28}$$

In practice, because of the small filter thickness and large V-panel spacing,

turbulent flow develops between the V-panels. The pressure drop caused by the V-panel structure can be corrected by considering the inlet and outlet effects [23]. These effects can be calculated for the filter by means of the local pressure drop formula from the field of fluid mechanics:

$$\Delta p_{in} = \xi_{in} \frac{\rho V_{in}^2}{2} \tag{29}$$

$$\Delta p_{out} = \xi_{out} \frac{\rho V_{out}^2}{2} \tag{30}$$

where

$\xi_{in} = 0.5\left(1 - \frac{A_{in}}{A_{cs}}\right)$, inlet local resistance coefficient

$\xi_{out} = \left(1 - \frac{A_{out}}{A_{cs}}\right)^2$, outlet local resistance coefficient

$V_{in} = \frac{Q}{A_{in}}$, filter inlet velocity

$V_{out} = \frac{Q}{A_{out}}$, filter outlet velocity

Here A_{cs}, A_{in}, A_{out} are the cross-sectional area, inlet area and outlet area of the filter, respectively.

Thus, we have obtained the pressure drop expression for each part of the multi-V cabin filter. By bringing the pressure drops of the five parts into Eq. (1), we can determine the pressure drop of the multi-V cabin filter. The empirical equation is too complicated to be displayed here. We can easily solve this formula with commonly used software, such as EXCEL or MATLAB.

2.2 CFD simulations

For the solution of $v_{x,dw}^*$ and $v_{y,dw}^*$, we used CFD to accurately calculate the flow field between the pleats, and converted it into a mathematical expression. The study was based on recommendations from the investigation of CFD use in simulating the airflow and pressure drop through a pleated filter system by Feng et al. [20]. Our simulations were conducted with the use of a commercial CFD program, ANSYS Fluent 17.0 [28]. The v2f turbulence model was used to predict the flow field between pleats. Because of the bounded porous wall flow characteristic in pleated filters, the v2f model can provide good results [20]. The porous media model in ANSYS Fluent was used for predicting the pressure drop through the filter medium. The flow in the porous medium was considered laminar.

We established two-dimensional models for the triangular and rectangular pleats with physical model parameters from Feng [29]. The filter-structure parameters are s = 0.38 mm, Y = 4 mm, L = 52 mm, and k = 1.22×10^{-12} m^2. Fig. 3 shows the computational domains and boundary conditions. The entrance velocity was the face velocity of the filter at U = 0.83 m/s. A two-dimensional grid was used to divide the flow domain to simulate flow through the pleats under steady-state conditions. We used a structured grid for the rectangular pleats and a quadrilateral unstructured grid

for the triangular pleats.

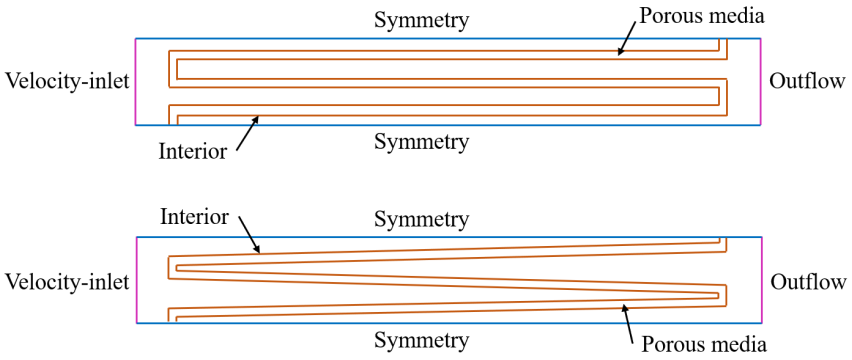

Fig. 3. Computational domains and boundary conditions for the rectangular and triangular pleats.

In our simulation, the SIMPLE algorithm was utilized in the pressure correction equation. The pressure discretization scheme used the standard first-order upwind, and all the others used the second-order upwind. In order to verify the accuracy of the simulation, we compared the pressure simulation results with the experimental values, as discussed in Section 3.1.

2.3 Experimental test rig and test procedure

We need to measure the pressure drop across the multi-V cabin filter to verify the accuracy of the empirical equation developed in Section 2.1. The pressure drop test used a HEPA filter test rig as shown in Fig. 4. It consisted of several square duct sections with internal dimensions of 610 mm × 610 mm. The airflow rate was controlled through adjustments of the fan speed to meet the requirements of the filter pressure drop tests. There were four static pressure taps at the peripheries of the upstream and downstream ducts, respectively, and the taps were connected together by a ring line to measure the pressure across the filter. Although this study only measured airflow rates and pressure drops, the experimental facility can also be used to test the filtration efficiency according to BS EN ISO 29463-5 [30] and the dust holding capacity of air filters according to EN 779 [31].

We tested the pressure drop across the filter at 50%, 75%, 100% and 125% rated airflow rates. This range was selected to cover the most likely recirculated airflow rates under actual flying conditions. The actual airflow rate through the filters varied because of the inconsistent engine power and uncontrolled recirculated air system pressure drop [32]. Since the external dimensions of the filter and the size of the duct were very different, it was necessary to construct the corresponding fixture (as shown in Fig. 5(b)) or to reduce the duct size for different filters, and to secure the filter in the duct for testing. Thus, the procedure for the pressure drop tests was as follows: (1) test the fixture pressure drop under different airflow rates, (2) secure the filter in the fixture and measure the pressure drop across the filter under different airflow rates, and (3) subtract the pressure drop for the fixture alone from that for the fixture with the filter, to obtain the actual pressure drop across the filter.

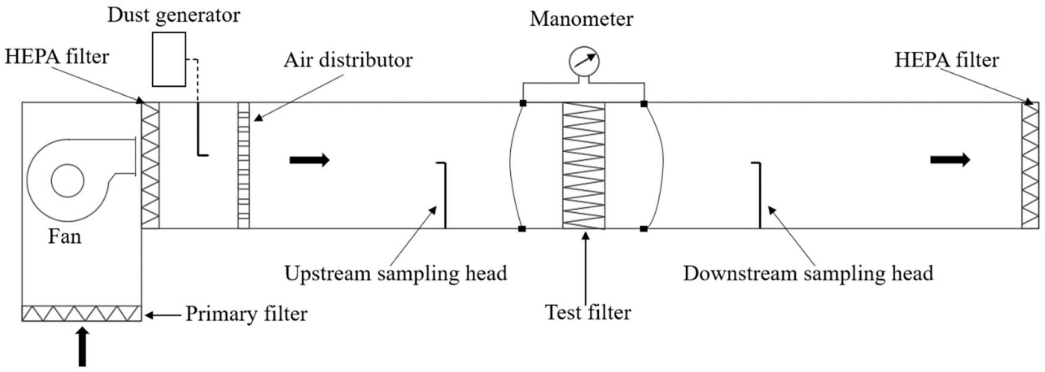

Fig. 4. Schematic of experimental test rig.

We tested six different types of multi-V cabin HEPA filters (as shown in Fig. 5(a)) in this investigation. They represented the filters used in five common Boeing aircraft models. Table 1 lists the parameters of the cabin filters, of which P199000 and 21FA413G were for different models of B747. Filters 21FA414 and P512777 were interchangeable parts for the same models of B777. The measurements indicated that the filters for different aircraft models have different structural parameters, but the mini-pleat height and spacing were the same (23 mm and 2.4 mm, respectively). The filtration area was calculated by multiplying the number of pleats by the surface area of one pleat. All filters were made of glass fiber medium.

(a) (b)

Fig. 5. Multi-V cabin HEPA filters: (a) 7600002-101 cabin filter for B737, (b) 21FA414 cabin filter for B777 with fixture

Table 1

Geometrical characteristics of multi-V cabin HEPA filters.

Filter part number	Manufacturer	Aircraft type	Q (m^3/h)	Length (mm)	Width (mm)	Thickness (mm)	Mini-pleat panel number	Mini-pleat panel spacing (mm)	Mini-pleat height (mm)	Mini-pleat length (mm)	Mini-pleat spacing (mm)	Filtration area (m^2)
7600002-101	PTI	B737& B757	2040	508	508	140	12	78	24	494	2.4	15.65
P199000	Donaldson	B747	1700	592	592	150	14	83	25	580	2.5	18.27
21FA413G	Purolator	B747	884	505	404	95	14	71	24	388	2.3	9.50
P512763	Donaldson	B767	2550	710	709	99	20	70	25	700	1.8	26.88
21FA414	Keddeg	B777	969	472	506	125	10	94	23	496	2.6	10.42
P512777	Donaldson	B777	969	475	507	125	10	94	25	497	2.5	11.93

3. Results

3.1 CFD simulations

Our purpose in using CFD was to solve $v^*_{x,dw}$ and $v^*_{y,dw}$, but we first needed to verify that the simulation results were correct. We compared the simulated filter pressure drop with the pressure drop measured by Feng [29]. There was no obvious difference in filter pressure drop between the two different pleat shapes when the pleat spacing and pleat height remained unchanged (rectangular pleat was 183 Pa, triangular pleat 188 Pa). The calculated pressure drop was close to the experimental value of 196 Pa, and thus the CFD results were validated.

We analyzed the flow fields of the rectangular and triangular pleats separately in order to facilitate the development of the empirical equations for $v^*_{x,dw}$ and $v^*_{y,dw}$. Fig. 6 shows the simulated velocity distribution in the downstream gap for the rectangular-pleat filter. The velocity component in the x direction was a quadratic function, and v_x increased uniformly along the airflow direction. The velocity component in the y direction was a cubic function. The inlet had an effect on the y-component velocity, and the remaining positions were independent of x.

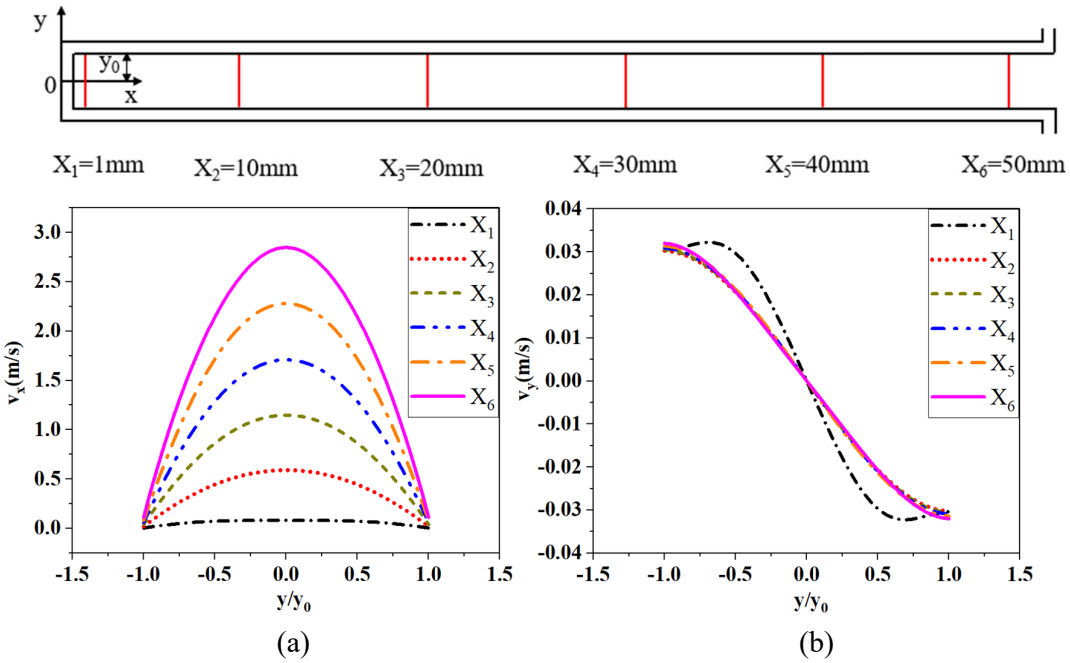

Fig. 6. Velocity distribution in the downstream gap of the rectangular pleat: (a) x-component velocity and (b) y-component velocity

Fig. 7 depicts the simulation results for the triangular-pleat filter. Note that v_x increased non-uniformly along the airflow direction. Because the H at the top of the pleat was very small, the y-component of velocity was approximately linear. The outlet at the gap had an effect on y-component velocity. The remaining positions were approximately independent of x. For the low-permeability HEPA filter medium, the

airflow between the pleats took the form of a laminar parabola.

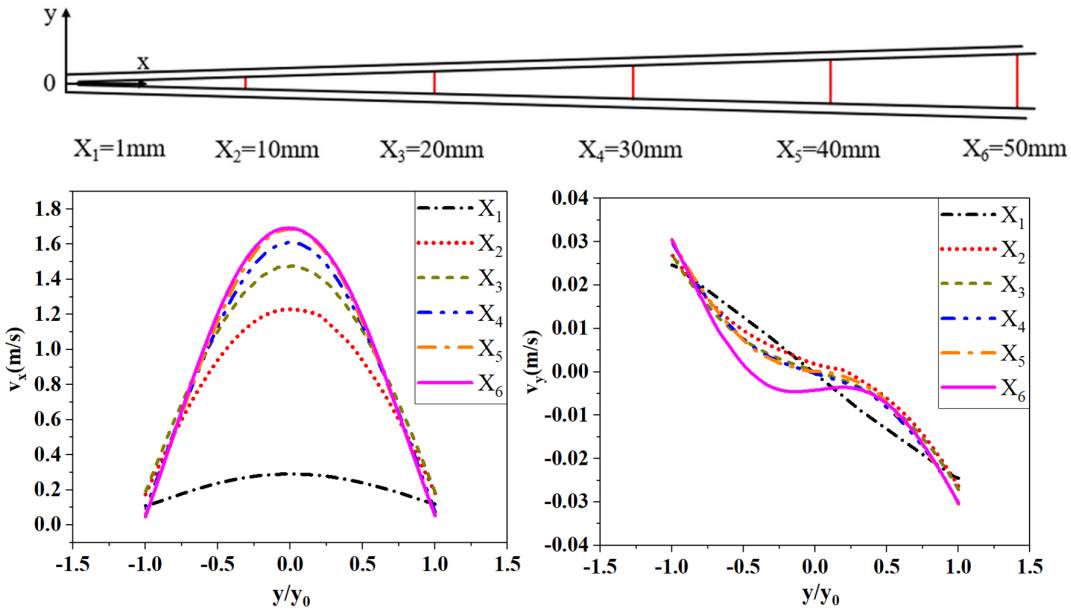

Fig. 7. Velocity distribution in the downstream gap of the triangular pleat: (a) x-component velocity and (b) y-component velocity

3.2 Verification of the empirical equations

This investigation used the measured pressure drop to verify the accuracy of the empirical equations. When the experimental airflow rate, the structural parameters of the filter and the performance parameters of the filter medium were introduced into the equations, the pressure drop through the filter under the corresponding airflow rate could be calculated. The performance parameters of the filter medium used in the calculations were k = 1.03×10^{-12} m^2 and s = 0.38 mm [17]. The selection basis of the parameters was that the filtration performance was consistent with the tested filters. Since the cabin filters had the same filtration efficiency rating, we used the same filter medium parameters for the calculations. Table 2 compares the calculated and measured pressure drop for filter P199000 under different flow rates. The empirical equations calculated the pressure drop with reasonable accuracy, with relative error of no more than 4.25%. The results also show that the pressure drop across the filter medium was a main part. The pressure drops for individual parts of the filter increased with the flow rate.

Table 2

Comparison of measured and calculated pressure drop for the P199000 filter.

Q (m^3/h)	$\Delta p_{in} + \Delta p_{out}$ (Pa)	Δp_{vp} (Pa)	Δp_{mp} (Pa)	Δp_m (Pa)	Δp_t (Pa)	Experimental (Pa)	Relative error
850	1.03	3.59	2	66	73	72	-1.38%
1275	2.33	8.05	4	99	113	116	2.36%

1700	4.14	14.29	6	132	156	163	4.25%
2125	6.46	22.31	8	165	201	209	3.64%

Next, Fig. 8 compares the measured and calculated pressure drop for the remaining cabin filters used in this investigation. The calculated pressure drop differed from the measured one by 7.84% on average. The results demonstrate that the empirical equations were sufficiently accurate in predicting the pressure drop across a multi-V filter.

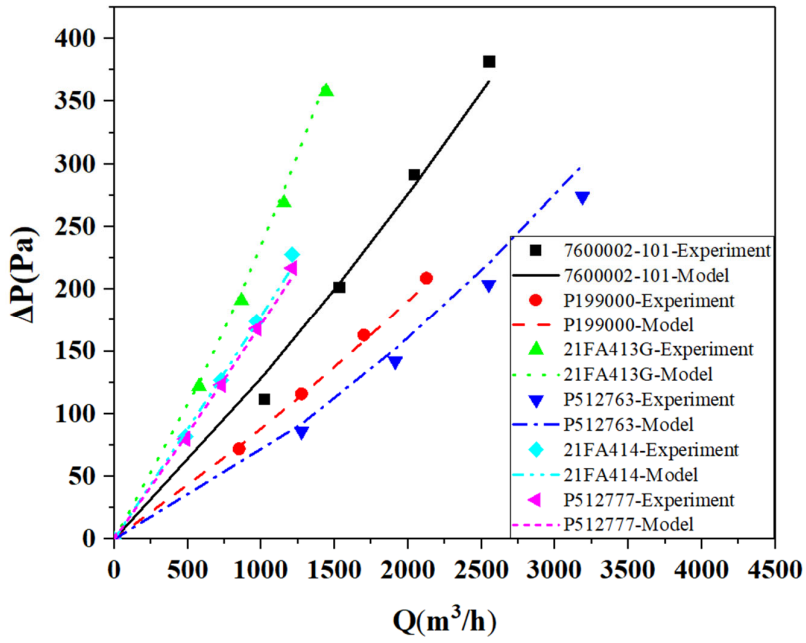

Fig. 8. Comparison of the measured and calculated pressure drop through different multi-V cabin filters

The $\Delta p_{mp} + \Delta p_m$ empirical equations can also be used to solve the pressure drop across pleated filter panels. We used the equations to calculate the pressure drop across an industrial HEPA pleated filter and compared the results with the experimental data obtained by Feng [29]. Our calculation used the following filter structure parameters: s = 0.38 mm, Y = 3.7 mm, L = 52 mm, and k = 1.22×10^{-12} m^2. As shown in Table 3, the calculated pressure drop agreed well with the experimental data, with a maximum relative error of 6.5%. These results further confirmed the accuracy of the empirical equations.

Table 3

Comparison of the measured and calculated pressure drop for a pleated filter panel with experimental data from Feng [29]

Q (m^3/h)	Δp_{mp} (Pa)	Δp_m (Pa)	Δp_t (Pa)	Experimental (Pa)	Relative error

850	9	142	151	162	6.50%
1000	12	167	179	187	4.35%
1250	17	209	226	230	1.83%
1500	22	251	273	273	0.00%
1700	27	285	312	308	-1.31%

We also compared the CFD simulated and the empirical formula calculated pressure drop for each part of pleated filter panels. Under the same conditions, the pressure drop in the mini-pleat flow channel Δp_{mp} calculated by the empirical formula and the CFD simulation was 11 Pa and 10 Pa, respectively. The pressure drop across the filter medium Δp_m calculated by the empirical formula was 181 Pa, while the CFD simulation result shows that the Δp_m was 173 Pa. The relative error was only 4.6%. Overall, our empirical formula calculation results were in good agreement with the above experimental values and simulation results.

3.3 Structural optimization for multi-V filters

The validated empirical equations can be a useful tool for optimizing the structural parameters of multi-V cabin filters. This section describes the optimization process.

The structural parameters are mini-pleat height, mini-pleat spacing, mini-pleat panel spacing and filter thickness. Let us use the P199000 multi-V cabin filter as an example. Fig. 9a illustrates the effect of mini-pleat spacing on the pressure drop across the filter. The pressure drop across the filter medium Δp_m gradually decreases as the mini-pleat spacing becomes smaller, because the narrower spacing increases the filtration area of the filter and reduces the filtration velocity. However, as the mini-pleat spacing becomes smaller, the pressure drop in the mini-pleat flow channel Δp_{mp} will gradually increase. This finding is the same as that of most studies on structure optimization of pleated filters [17-19, 22-25]. Therefore, at a certain mini-pleat height, there is a mini-pleat spacing that minimizes the filter pressure drop. In the multi-V cabin filter, the change in the mini-pleat spacing has no effect on the pressure drop across the V-panel structure.

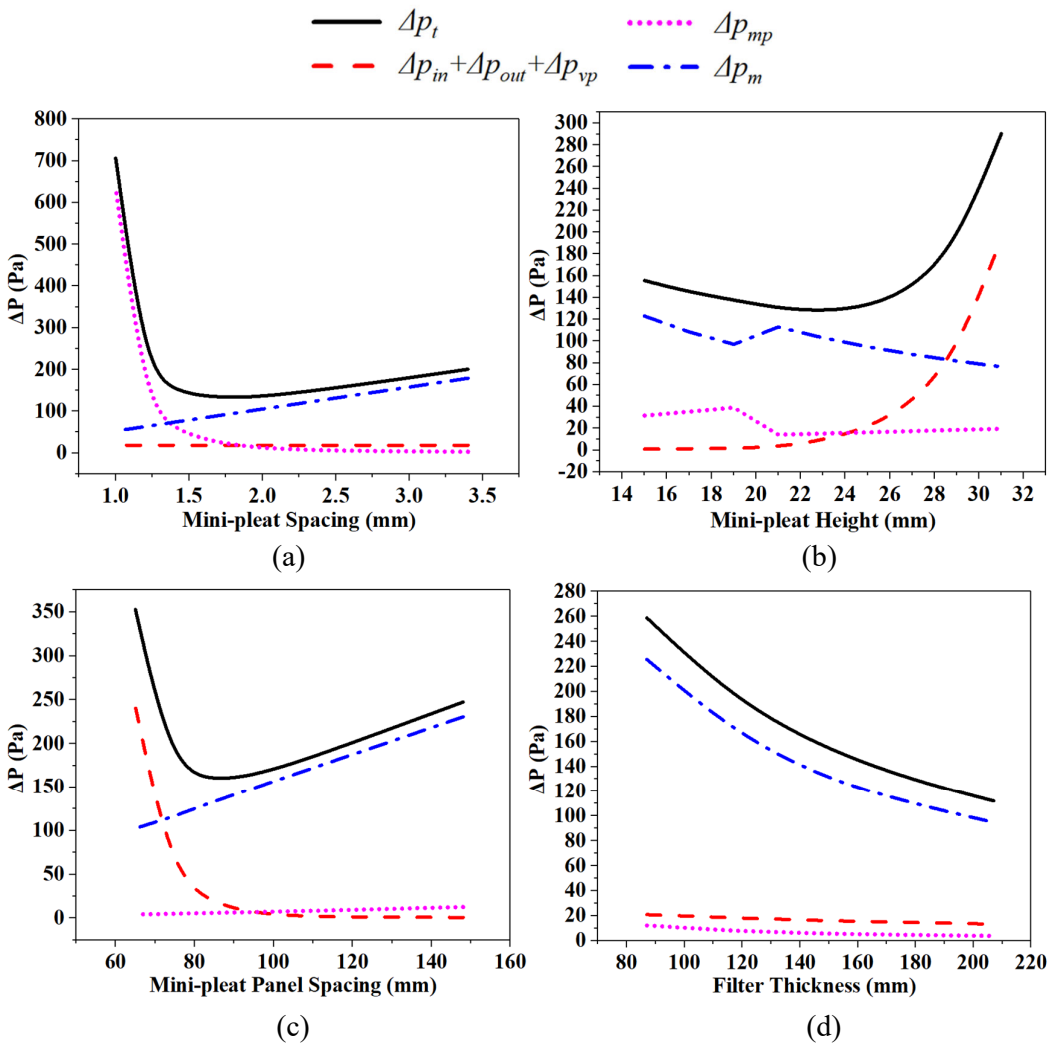

Fig. 9. The influence of different structural parameters on the filter pressure drop: (a) mini-pleat spacing, (b) mini-pleat height, (c) mini-pleat panel spacing, and (d) filter thickness

Fig. 9b depicts the effect of mini-pleat height on pressure drop. When the height ranged from 15 to 19 mm and from 20 to 31 mm, respectively, the corresponding optimal mini-pleat spacings were 1.4 mm and 1.8 mm. Therefore, the pressure drop across the filter medium Δp_m and the pressure drop in the mini-pleat flow channel Δp_{mp} exhibited a step at the mini-pleat height of about 20 mm. Under the same mini-pleat spacing, an increase in mini-pleat height made the filtration area larger and the pressure drop across the filter medium Δp_m smaller. However, the increase in mini-pleat height also led to a greater pressure drop in the mini-pleat flow channel Δp_{mp}, and could reduce the height of the channel between the mini-pleat panels, thereby increasing the pressure drop across the V-panel structure, $\Delta p_{in} + \Delta p_{out} + \Delta p_{vp}$. Thus, the filter had an optimal mini-pleat height.

Fig. 9c illustrates the influence of V-panel structure on different components of the pressure drop. The figure reveals an optimal mini-pleat panel spacing, at which the

pressure drop across the filter was the lowest. Since external dimensions are fixed, a reduction of the distance between mini-pleat panels allows an increase in the number of panels, thereby increasing the filtration area and reducing the pressure drop across the filter medium Δp_m. In addition, increasing the number of mini-pleat panels can reduce both the face velocity of the mini-pleat panel and the pressure drop in the mini-pleat flow channel Δp_{mp}. However, reducing the distance between mini-pleat panels would increase the pressure drop across the V-panels structure $\Delta p_{in} + \Delta p_{out} + \Delta p_{vp}$. These observations explain the optimal mini-pleat panel spacing.

According to Fig. 9d, the effect of filter thickness on the pressure drop is different from the effects of the other three parameters. The pressure drop across the filter decreases as the thickness increases. This is because, as the thickness increases, the filtration area increases and the pressure drop across the filter medium Δp_m becomes smaller. Similarly, increasing the thickness can increase the windward area of the mini-pleat panels, thereby reducing the pressure drop in the mini-pleat flow channel Δp_{mp}. Since both sides of the filter are in the form of openings, as the thickness increases, the inlet velocity of the filter will decrease. Thereby the pressure drop across the V-panel structure $\Delta p_{in} + \Delta p_{out} + \Delta p_{vp}$ is reduced. However, one could not reduce the pressure drop across the filter by increasing the thickness indefinitely. This is because an airliner cabin filter must be lightweight with good shock resistance. The filter thickness needs to be limited so that the filter can be fixed securely in the duct of the environmental control system. In addition, according to our calculations, different filter thicknesses had the same optimal mini-pleat panel spacing. Therefore, the mini-pleat panel spacing was determined only by the mini-pleat height.

The above results indicate that when the mini-pleat height is known, the corresponding mini-pleat spacing and mini-pleat panel spacing in the filter can be determined. Fig. 10 displays two design optimization procedures for multi-V cabin filters. The first procedure starts with mini-pleat height, and the second starts with mini-pleat panel spacing. Our optimal design also considered the following two factors. First, due to technical limitations in the manufacturing process, the minimum mini-pleat height would be 23 mm. Second, to account for dust holding, the actual mini-pleat spacing should be slightly larger than the calculated optimal mini-pleat spacing [23,34]. Our optimization design principle for multi-V cabin filter was to increase the filtration area as much as possible without affecting the structural resistance of the filter, thereby reducing the filtration velocity. A lower filtration velocity would not only reduce the pressure drop of the filter, but also enable the filter to obtain higher filtration efficiency.

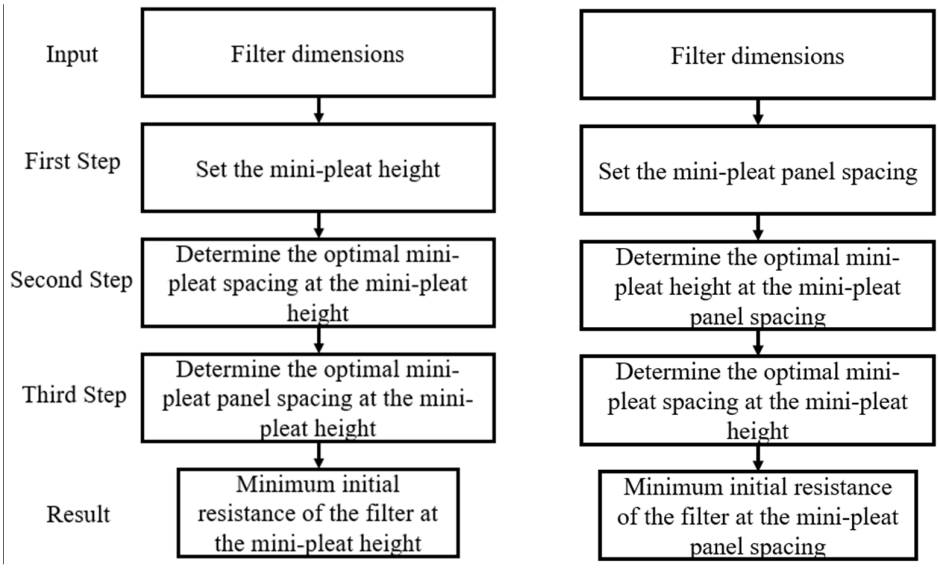

(a) (b)

Fig. 10. Two design optimization procedures for multi-V cabin filters

Taking the P199000 filter as an example, the two design procedures led to the results shown in Tables 4 and 5, respectively. The optimal structural parameters obtained by the two design procedures are the same. The actual parameters of the filter shown in Table 1 are very close to the optimal ones. We believe the filter manufacturers had optimized their designs, and our results confirmed their good designs.

Table 4

Optimal parameters of the P199000 filter obtained by the first design optimization procedure

Mini-pleat height (mm)	Mini-pleat spacing* (mm)	Mini-pleat panel spacing (mm)	$\Delta p_{in} + \Delta p_{out}$ (Pa)	Δp_{vp} (Pa)	Δp_{mp} (Pa)	Δp_m (Pa)	Δp_t (Pa)
5	1.7	19	4.02	9.37	1	103	117
10	1.9	37	3.41	6.54	2	111	123
15	1.9	53	3.81	10.02	5	108	127
20	2.3	74	3.06	4.96	5	134	148
23	2.3	84	3.19	5.95	7	134	150
24	**2.3**	**84**	**3.77**	**10.16**	**7**	**128**	**149**
25	2.3	84	4.47	16.11	7	123	151
30	2.3	98	5.03	21.81	10	119	157
35	2.3	118	4.38	15.70	15	123	158

*The calculated optimal mini-pleat spacing was increased by 0.5 mm for dust holding.

The bold font indicates optimal structural parameters.

Table 5

Optimal parameters of the P199000 filter obtained by the second design optimization procedure

Mini-pleat panel spacing (mm)	Mini-pleat panel Number	Mini-pleat height (mm)	Mini-pleat spacing* (mm)	$\Delta p_{in} + \Delta p_{out}$ (Pa)	Δp_{vp} (Pa)	Δp_{mp} (Pa)	Δp_m (Pa)	Δp_t (Pa)
45	26	11	1.9	2.29	0.43	3	124	130
49	24	13	1.9	3.00	4.31	4	114	125
53	22	13	1.9	2.26	0.39	5	124	132
59	20	15	1.9	2.51	1.69	6	118	129
65	18	17	1.9	2.75	3.05	7	116	129
74	16	19	1.9	2.54	1.96	9	117	131
84	**14**	**24**	**2.3**	**3.77**	**10.16**	**7**	**128**	**149**
98	12	27	2.3	3.26	6.46	10	133	152
118	10	31	2.3	2.75	3.17	13	139	158

*The calculated optimal mini-pleat spacing was increased by 0.5 mm for dust holding.

The bold font indicates optimal structural parameters.

This investigation optimally designed the other filters that were studied, and Table 6 shows the results of the design process. Again, most of the optimal structural parameters for the filters were very close to the actual parameters shown in Table 1. According to the optimization results, filter 7600002-101 for the B737 aircraft can attain a lower pressure drop in the case of 12 and 14 mini-pleat panels. Similarly, filter P512763, used in the B767 aircraft, exhibited a lower pressure drop in the case of 18 and 20 mini-pleat panels. In addition, the research results show that the filters 21FA414 and P512777 of the B777 aircraft had a lower initial pressure drop when the number of mini-pleat panels was increased to 12.

Table 6

Design optimization for geometrical characteristics of multi-V cabin filters

Filter part number	Aircraft type	Q (m^3/h)	Length (mm)	Width (mm)	Thickness (mm)	s (mm)	k (m^2)	Mini-pleat height (mm)	Mini-pleat spacing (mm)	Mini-pleat panel number	Mini-pleat panel spacing (mm)	Δp_t (Pa)
7600002-101	B737& B757	2040	508	508	140	0.38	1.03E-12	25	2.3	12	84	255
								23	2.3	14	72	255
P199000	B747	1700	592	592	150	0.38	1.03E-12	24	2.3	14	84	149
21FA413G	B747	1155	505	404	95	0.38	1.03E-12	23	2.3	14	72	265
P512763	B767	2550	710	709	99	0.38	1.03E-12	23	2.3	20	71	223
								24	2.3	18	78	223
21FA414	B777	969	472	506	125	0.38	1.03E-12	23	2.3	12	79	149
P512777	B777	969	475	507	125	0.38	1.03E-12	23	2.3	12	79	149

4. Discussion

The empirical model performed quite well in predicting pressure drop across complex multi-V filters. However, the model had some limitations:

- The pressure drop simulation results for pleated filter panels were basically the same as the experimental data, but there were still some deviations. Possible reasons for the deviations between the experimental and calculated pressure were: (1) There was a measurement error in the pressure drop that was inevitable. (2) In the modeling, we set the zone at the top of the pleat as porous medium, but in practice, due to the medium was heavily compressed, only a small amount of fluid enters the pleat at the top. This may also cause the discrepancy between the simulated and empirical formula results. (3) The setting of the porous media parameters in CFD may bring errors. In practice, the permeability of the porous media may not be constant [38,39], and there is a deviation between the filter media permeability measured and calculated through experiments and the actual permeability.
- This study used the same parameters of filter material performance for all the studied filters, but there are actually slight differences. However, it is difficult to obtain the parameters because they are commercial secrets. Therefore, for different materials, one should use our model with caution.
- This model only predicts pressure drop through a clean filter. During the dust-holding process, the pressure drop through the filter is complicated. To date, most studies have used CFD simulations and semi-empirical formulas to study the effects of the filter dust-holding process on pressure drop and filtration efficiency [33-37]. The results show that increasing the pleat density can increase the dust holding capacity. The development of a model to predict the pressure drop due to dust holding will be addressed in a future effort. Our prediction of the initial pressure drop of the cabin filter also formed the basis for the subsequent full-cycle pressure drop prediction.
- Our empirical equations were built on the basis of the multi-V HEPA filters used in commercial airplanes. The model had high accuracy for filters constructed with low-permeability media. In fact, multi-V filters are widely used in other industries, but the specific form is slightly different. Whether this empirical formula can be extended to other multi-V filters remains to be studied.

5. Conclusions

This investigation proposed an empirical model to predict the different components of the pressure drop through the type of multi-V HEPA filter used in commercial airplanes. The model's development was aided by CFD simulations of two-dimensional airflow and pressure drop through triangular and rectangular pleats. This study also measured the pressure drop through multi-V HEPA cabin filters, and the experimental data was used to verify the accuracy of the empirical model. The calculated pressure drop differed from the measured data by 7.84% on average for the filters studied. Thus, the proposed empirical model is sufficiently accurate.

By using the empirical model to study the structural parameters of the multi-V HEPA cabin filters, this study found that optimal parameters existed for mini-pleat panel spacing, number of mini-pleat panels, mini-pleat height, and mini-pleat spacing. The minimum mini-pleat height will be dependent on the manufacturing technique, and mini-pleat spacing should include space for dust holding.

This study also proposed two design optimization procedures for multi-V HEPA cabin filters. The aim was to design the structural parameters of the filters to provide the lowest pressure drop and highest filtration efficiency. The results obtained by the two design

procedures are the same, and are very close to the actual parameters of commercial filters that should have been optimized by their manufacturers.

Acknowledgement

This study was supported by the National Key R&D Program of the Ministry of Science and Technology, China, on "Green Buildings and Building Industrialization" through Grant 2018YFC0705300.

References

[1] X. Xie, Y. Li, H. Sun, L. Liu, Exhaled droplets due to talking and coughing, J. R. Soc. Interface 6 (2009).

[2] J.D. Noti, F.M. Blachere, C.M. McMillen, W.G. Lindsley, M.L. Kashon, D.R. Slaughter, D.H. Beezhold, High humidity leads to loss of infectious influenza virus from simulated coughs, PLoS One 8 (2013) e57485.

[3] G.R. Johnson, L. Morawska, The mechanism of breath aerosol formation, J. Aerosol Med. Pulm. D. 22 (2009) 229-237.

[4] John D. Spengler, E.M. Jose Vallarino, H. Estephan, In-Flight/Onboard Monitoring: ACER's Component for ASHRAE 1262, Part 2, (2012).

[5] A.C. Rai, C. Lin, Q. Chen, Numerical modeling of particle generation from ozone reactions with human-worn clothing in indoor environments, Atmos. Environ. 102 (2015) 145-155.

[6] Z. Li, J. Guan, Xudong Yang, C. Lin, Source apportionment of airborne particles in commercial aircraft cabin environment: Contributions from outside and inside of cabin, Atmos. Environ. 89 (2014) 119-128.

[7] Q. Cao, Y. Liu, W. Liu, C. Lin, D. Wei, S. Baughcum, S. Norris, X. Shen, Z. Long, Q. Chen, Experimental study of particle deposition in the environmental control systems of commercial airliners, Build. Environ. 96 (2016) 62-71.

[8] C.I. Davidson, R.F. Phalen, P.A. Solomon, Airborne particulate matter and human health: A review, Aerosol Sci. Tech. 39 (2005) 737-749.

[9] W. Glover, H. Chan, S. Eberl, E. Daviskas, J. Verschuer, Effect of particle size of dry powder mannitol on the lung deposition in healthy volunteers, Int. J. Pharmaceut. 349 (2008) 314-322.

[10] J.O. Anderson, J.G. Thundiyil, A. Stolbach, Clearing the air: A review of the effects of particulate matter air pollution on human health, Journal of Medical Toxicology 8 (2012) 166-175.

[11] P. Møller, J.K. Folkmann, L. Forchhammer, E.V. Bräuner, P.H. Danielsen, L. Risom, S. Loft, Air pollution, oxidative damage to DNA, and carcinogenesis, Cancer Lett. 266 (2008) 84-97.

[12] J.W. Tang, Y. Li, I. Eames, P.K.S. Chan, G.L. Ridgway, Factors involved in the aerosol transmission of infection and control of ventilation in healthcare premises, J. Hosp. Infect. 64 (2006) 100-114.

[13] J.F. Chan, S. Yuan, K. Kok, K.K. To, H. Chu, J. Yang, F. Xing, J. Liu, C.C. Yip, R.W. Poon, H. Tsoi, S.K. Lo, K. Chan, V.K. Poon, W. Chan, J.D. Ip, J. Cai, V.C. Cheng, H. Chen, C.K. Hui, K. Yuen, A familial cluster of pneumonia associated with the 2019 novel coronavirus indicating person-to-person transmission: a study of a family cluster, The Lancet 395 (2020) 514-523.

[14] M.B. Hocking, Passenger aircraft cabin air quality: trends, effects, societal costs, proposals, Chemosphere 41 (2000) 603-615.

[15] ANSI/ASHRAE Standard 161. Air Quality within Commercial Aircraft. American Society of Heating, Refrigerating and Air-Conditioning Engineers, Atlanta. 2013

[16] K. Bull, Cabin air filtration: Helping to protect occupants from infectious diseases, Travel Med. Infect. Di. 6 (2008) 142-144.

[17] D. Chen, D.Y.H. Pui, B.Y.H. Liu, Optimization of pleated filter designs using a finite-element numerical model, Aerosol Sci. Tech. 23 (1995) 579-590.

[18] L. Del Fabbro, J.C. Laborde, P. Merlin, L. Ricciardi, Air flows and pressure drop modelling for different pleated industrial filters, Filtr. Separat. 39 (2002) 34-40.

[19] P. Tronville, R. Sala, Minimization of resistance in pleated-media air filter designs: Empirical and CFD approaches, HVAC&R Research 9 (2003) 95-106.

[20] Z. Feng, Z. Long, Q. Chen, Assessment of various CFD models for predicting airflow and pressure drop through pleated filter system, Build. Environ. 75 (2014) 132-141.

[21] F. Théron, A. Joubert, L. Le Coq, Numerical and experimental investigations of the influence of the

pleat geometry on the pressure drop and velocity field of a pleated fibrous filter, Sep. Purif. Technol. 182 (2017) 69-77.
[22] H.H.S.Y. GOULDING, Optimized ultra high efficiency filter for highefficiency industrial combustion turbines, ASME International Gas Turbine and Aeroengine Congress and Exhibition, Koln, 1992.
[23] T. Lücke, H. Fissan, The prediction of filtration performance of high efficiency gas filter elements, Chem. Eng. Sci. 51 (1996) 1199-1208.
[24] D.R.D.Y. Chen, D.Y.H. Pui, Y.M. Tang, Filter Pleating Design for Cabin Air Filtration, (1996).
[25] M. Rebaï, M. Prat, M. Meireles, P. Schmitz, R. Baclet, A semi-analytical model for gas flow in pleated filters, Chem. Eng. Sci. 65 (2010) 2835-2846.
[26] F. Hai-ming, X. Fang, J. Ruifang, Relationship of filtration resistance with geometry parameters across pleated aerosol filter, Journal of Huaqiao University(Natural Science) 31 (2010) 307-312.
[27] R. Adam, T. Lücke, Der Druckverlust von Filterelementen für die Schwebstoffiltration, Staub. Reinhaltung der Luft 54 (1994) 247-252.
[28] ANSYS Inc.. ANSYS Fluent 17.0 User's Guide. ANSYS Inc. Southpointe. 2015.
[29] Z. Feng, Experimental study of relationship between resistance and structure of high efficiency particulate air Filter, MA.Eng. Thesis, Tsinghua University (in Chinese). 2007.
[30] EN BS ISO 29463-5. High-efficiency filters and filter media for removing particles in air. Brussels: CEN. 2018.
[31] EN 779. Particle air filters for general ventilation-determination of filtration performance. Brussels: CEN. 2012.
[32] B. Xu, J. Liu, S. Ren, W. Yin, Q. Chen, Investigation of the performance of airliner cabin air filters throughout lifetime usage, Aerosol Air Qual. Res. 13 (2013) 1544-1551.
[33] L. Del Fabbro, P. Brun, J.C. Laborde, J. Lacan, A. Renoux, L. Ricciardi, Study of the clogging of industrial pleated filters by solid particles, J. Aerosol Sci. 31 (2000) 210-211.
[34] S. Fotovati, S.A. Hosseini, H. Vahedi Tafreshi, B. Pourdeyhimi, Modeling instantaneous pressure drop of pleated thin filter media during dust loading, Chem. Eng. Sci. 66 (2011) 4036-4046.
[35] S. Fotovati, H.V. Tafreshi, B. Pourdeyhimi, A macroscale model for simulating pressure drop and collection efficiency of pleated filters over time, Sep. Purif. Technol. 98 (2012) 344-355.
[36] A.M. Saleh, S. Fotovati, H. Vahedi Tafreshi, B. Pourdeyhimi, Modeling service life of pleated filters exposed to poly-dispersed aerosols, Powder Technol. 266 (2014) 79-89.
[37] A.M. Saleh, H. Vahedi Tafreshi, A simple semi-numerical model for designing pleated air filters under dust loading, Sep. Purif. Technol. 137 (2014) 94-108.
[38] L. Lo, S. Hu, D. Chen, D.Y.H. Pui, Numerical study of pleated fabric cartridges during pulse-jet cleaning, Powder Technol. 198 (2010) 75-81.
[39] J. Li, P. Wang, D. Wu, D. Chen, Numerical study of opposing pulsed-jet cleaning for pleated filter cartridges, Sep. Purif. Technol. 234 (2020) 116086.